JOURNAL OF AIRCRAFT
Vol. 47, No. 4, July–August 2010

Low-Reynolds-Number Airfoil Investigation of Lower-Surface Leading-Edge Flaps

Lance W. Traub* and Sreyes Kadapala†
Embry-Riddle Aeronautical University, Prescott, Arizona 86301

DOI: 10.2514/1.C031006

A low-speed wind-tunnel investigation was undertaken to evaluate the ability of a small leading-edge flap attached to the pressure surface of a Clark Y airfoil to improve low-Reynolds-number performance. Different flap geometries and designs were evaluated. Testing encompassed the measurement of lift and drag, surface pressures, and surface-flow topology rendered using titanium dioxide. Tests were undertaken at Reynolds numbers of 75,000 and 150,000. The results show that the flaps shift the zero-lift angle of attack in the positive direction, with the lift decrement stemming from reduced lower-surface pressure. The flaps proved to be beneficial only at high angles of attack, where they cause a sustained lift plateau and eliminate hysteresis.

Introduction

THE proliferation of small-scale unmanned aerial vehicles (UAVs) has promulgated a significant research effort to enhance the performance of these aircraft. Complications arise in the typical Reynolds numbers of operation of these craft, often less than 200,000. At such operational conditions, efficient performance is constrained by Reynolds number effects [1]: premature separation, failure of boundary-layer transition mechanisms (and, consequently, reattachment), etc. As a result, lift is often limited and drag is excessive.

Performance degradation may be lessened by attention to airfoil design [2,3] or through the use of devices to cause transition or structured/controlled separation [4]. Efforts by Selig and Guglielmo [2], Eppler [5], and other researchers have yielded to the community a range of low-Reynolds-number airfoils with effective performance for $Re > 100,000$. Below 100,000, difficulty in enabling transition due to excessive laminar boundary-layer stability complicates effective airfoil design. A notable exception is the use of slender wings in the form of deltas [6], where enforced flow separation from the leading edge leads to a stable system of vortices that enhance lift and are relatively unaffected by Reynolds number. Unfortunately, deltas, in common with most slender wings, are poor lift generators and may not provide sufficient lift to sustain a UAV-type vehicle or may require excessive flight velocity.

An alternative approach to the innate airfoil design is to use devices to promote the desired flow effect. A recent study by Jones et al. [7] suggested that a small leading-edge feather employed by some birds may serve as a transition device that enables attached flow. Their results showed that the flap generated disturbances that convected over the upper surface of the test airfoil at high incidence and eliminated the formation of a laminar separation bubble. A study by Zhang and Zhou [8] showed that corrugations on the wing of a dragonfly may have the effect of generating a Kelvin–Helmholtz instability that propagates with the separating shear layer and promotes transition. A similar approach by Wong and Rinoie [9] used a small plate or block to institute the instability, with a moderate delay noted in the onset of stall.

Received 27 October 2009; revision received 28 December 2009; accepted for publication 6 January 2010.

*Associate Professor, Aerospace and Mechanical Engineering Department. Member AIAA.

†Undergraduate Student, Aerospace and Mechanical Engineering Department.

At low Reynolds numbers, transition is usually effected through the presence of a laminar transition bubble [10]. The bubble generally forms aft of the minimum-pressure point. The separated shear layer that forms its dividing stream surface usually transitions to turbulence due to high receptivity to disturbances and a lack of viscous wall damping. Mixing downstream of transition promotes shear-layer expansion and flow reattachment. If the bubble is small, it has a negligible effect on lift but increases drag, as the momentum thickness of the reattached turbulent boundary layer is greater than that due to an attached-flow transition process. Vortex generators [4,11] have been shown to potentially eliminate the bubble, but should be of minimal height to limit premature transition and thus extraneous drag due to excessive lengths of attached turbulent flow. As suggested by Kerho et al. [4], it may be optimal to use small vortex generators that diminish the size of the bubble without eliminating it totally.

An additional complication in low-Reynolds-number flows is the appearance of hysteresis in the lift, drag, and moment plots. Generally hysteresis is associated with different locations for the separation point during airfoil pitch-up and pitch-down. Concerns over the occurrence of hysteresis are associated with nonunique lift, drag, and lift-to-drag values. Typically, a clockwise hysteresis loop forms if a transition bubble appears at moderate incidence such that a relatively high maximum lift is produced [12]. A counterclockwise bubble may exist if flow separation occurs at low incidence without shear-layer transition or reattachment. At higher angles of attack, shear-layer transition results in turbulent attachment with an increase in lift, which is then maintained as the wing incidence reduces. Freestream turbulence has been shown to eliminate hysteresis [12].

Lower-surface leading-edge plates have been evaluated by Traub [13], Rinoie and Stollery [14], and Rao and Johnson [15] as a means of enhancing the performance of delta wings and delta wings with vortex flaps by augmenting and concentrating leading-edge vortex suction. The plate was constituted of a thin metal sheet attached below the leading edge and projecting out so as to be coincident with the leading edge when viewed from above. In that application, the plates appeared to improve wing performance.

Although the study by Jones et al. [7] appears to show benefit of the leading-edge flap as a transition device, little published information is available on similar implementations, especially at very low Reynolds numbers. Consequently, an experimental investigation has been undertaken to evaluate various leading-edge-flap geometries at low Reynolds numbers. Performance characterization includes force balance, pressure measurement, and flow visualization.

Equipment and Procedure

Wind-tunnel tests were conducted in Embry-Riddle University's 1 by 1 ft open-return facility. This wind tunnel has a measured

Table 1 Pressure-port locations

x/c	Locations along the chord length																			
u	0.03	0.05	0.08	0.1	0.13	0.15	0.2	0.25	0.3	0.35	0.4	0.45	0.5	0.55	0.60	0.65	0.7	0.75	0.8	0.85
l	0.05	0.13	0.22	0.3	0.39	0.47	0.56	0.64	0.73	0.81	——	——	——	——	——	——	——	——	——	——

turbulence intensity of 0.5% and jet uniformity within 1% in the core. The wall boundary layer is approximately 5 mm thick. Force measurements were taken using an in-house-designed and in-house-manufactured low-range platform balance. The balance has a maximum range of 43 N and a demonstrated accuracy, resolution, and repeatability of 0.0098 N. Angle setting ability is within 0.1 deg. Tests were conducted at Reynolds numbers of 75,000 and 150,000. A computer-controlled acquisition system was written for this balance using LabVIEW 8.2. Repeated force-balance data measurements in the attached-flow regime (4 deg incidence) and at stall (14 deg incidence) yielded an uncertainty for the lift and drag coefficients of 0.014 and 0.001 and 0.02 and 0.01 for a 95.5% probability, respectively.

Two wings were designed with CATIA software and then rapid-prototyped using Embry-Riddle's rapid-prototyping facilities, yielding ABS (acrylonitrile butadiene styrene) plastic wing representations. The wing chord c was 101.6 mm. One wing served for pressure measurement and the other served for force-balance tests. The wing section was a Clark Y. The profile was chosen due to its compatibility with the leading-edge plates; i.e., the section's flat bottom allows clean installation. The airfoil is also effective at low Reynolds numbers, as is documented in the Results and Discussion section. The tappings on the pressure-tapped wing were arranged in a diagonal at 20 deg to avoid causing transition. Thirty taps were used: 20 on the upper surface and 10 on the lower surface. The tubing used for the ports had an internal diameter of 0.8 mm. Care was taken to ensure that the taps were clean and did not protrude from the surface. The taps were formed by passing Tygon® tubing of the appropriate internal diameter through a preformed location hole in the rapid-prototyped wing surface. The tubing was then bonded in place on the inside of the wing and then cut to length using a thin blade held parallel to the surface. This method resulted in cleanly formed pressure taps that were flush with the surface. Locations of the pressure taps are given in Table 1, where x/c corresponds to locations along the chord length, and u and l correspond to the upper and lower surfaces, respectively. Pressure measurements were only conducted using the constant-chord (Fig. 1) leading-edge flaps with variable δ, as the triangular or cutout flaps would likely introduce three dimensional flow, leading to erroneous characterization, considering the pressure-tapping geometry.

Pressures were measured using an electronic pressure scanner. The scanner contains 30 independent temperature-compensated differential pressure transducers. The transducers are connected through solenoid valves to the measurement ports. An interface was written in Visual Basic to control the valves as well as to process and record the measured pressures. The valves were used to facilitate automatic zeroing of the transducers while running, eliminating any null or thermal offset effects. The pressure-transducer outputs were digitized using a 32-channel, 16-bit National Instruments external analog-to-digital converter board. The board allows scanning of the pressures at up to 250,000 readings/second. All presented pressures are the average of 1000 readings. Calibration of the scanner was performed using a FlowKinetics™ LLC FKT 1DP1A-SV pressure/flow meter. The FKT meter is calibrated against a deadweight primary standard and was within its calibration specifications. Comparison with the standard showed accuracy of better than 0.5 Pa. Calibration and comparison of the scanner with the FKT meter showed measured pressure agreement within 0.8 Pa for all 30 of the transducers. The tunnel freestream velocity was measured using a FlowKinetics LLC FKT 2DP1A-C meter. This meter measures atmospheric pressure, temperature, and relative humidity, all of which are used to compute the density used in the velocity calculation. Meter accuracy is specified by the manufacturer as better than 0.1%.

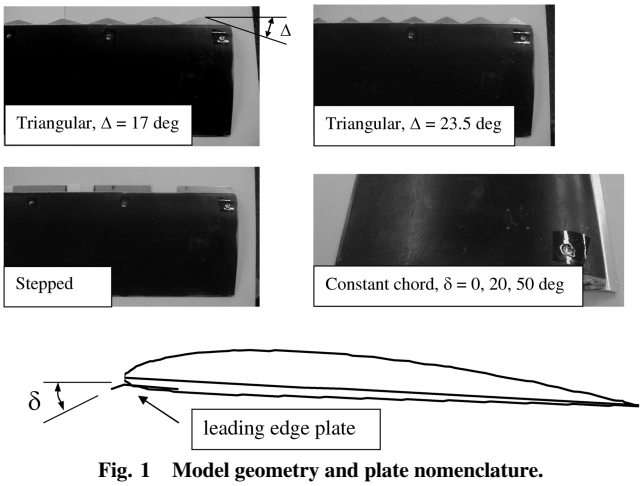

Fig. 1 Model geometry and plate nomenclature.

Six different leading-edge plate configurations were evaluated (see Fig. 1). In all instances, the flaps projected less than 6.25% chord beyond the leading edge. The plates were manufactured from 0.6-mm-thick aluminum sheet and attached to the lower wing surface using screws. The flaps separated from the lower airfoil surface at $x/c = 0.08$ and $y/c = -0.028$ with respect to the airfoil nose. Triangular, stepped, and constant-chord flap geometries were evaluated. The two-dimensional vortex formed above the constant-chord flaps (i.e., the flap chord does not change across the span, denoted as $\delta = 0$, 20, and 50 deg in this study, where δ is the flap angle) may be unstable (it would grow in time as fluid is fed in, but has no fluidic exit). Consequently, triangular-shaped flaps were also evaluated, as it may be expected that they would create discrete vortices over each segment. The triangular elements sweep angle Δ was dictated by the limited extent that the flaps projected beyond the leading edge. A high sweep angle would have caused a large number of triangular segments. Consequently, low sweep angles were (arbitrarily) selected to limit the number of elements but still initiate organized separation at high incidence.

A similar notion of the formation of discrete vortices suggested evaluating the effect of the stepped flaps. Both the stepped and triangular flaps were not inclined: i.e., $\delta = 0$ deg. The spanwise extent of the constant-chord flap segment for the stepped geometry was 0.53 c, and the gaps were 0.25 c. In most instances, the flap projected from 5 to 6.3 mm ahead of the airfoil's leading edge. As the flap may serve as a transition-type device, no trip strips or equivalent were used in the experiments. Because of the comparative nature of the tests, wall corrections were not applied. Force coefficients were nondimensionalized by the projected area of the airfoil and exposed flap area.

Crossflow and surface-flow visualization was performed using a mixture of titanium dioxide, paraffin, linseed oil, and oleic acid. As the models were mounted vertically, effects of gravity are eliminated on the crossflow. A splitter plate was manufactured to serve as the canvas for the crossflow. The wing was set at the desired angle of attack (AOA), the mixture was applied to the splitter plate using a brush, and the tunnel was increased to the desired Reynolds number rapidly. The fluid motion was observed to aid in interpretation. Surface visualization was undertaken for AOA = 10 and 22 deg. Testing was also performed with the model mounted horizontally to establish the surface-flow topology at angles of attack of 12, 22, 24, and 26 deg.

Results and Discussion

The low-Reynolds-number testing environment can be challenging due to the difficulty of obtaining representative loads when the

forces are very small. In addition to direct balance calibration, an indication of data quality may be ascertained from the ability of the facility to repeat runs showing close measurement accord. Figure 2a displays repeated data runs for the test Reynolds numbers of 75,000 and 150,000. All reported testing encompassed pitching the airfoil to approximately 18 deg in 2 deg increments followed by an incidence reduction (approximately 10 deg) to establish the presence and nature of the hysteresis loop. As may be seen, data repeatability is excellent with a clockwise hysteretic loop present for both Reynolds number cases. Although the applicability of using a Clark Y airfoil in the present study may appear dubious (or of limited utility), this section performs well, even at low Reynolds numbers. This is explored in Fig. 2b, where the measured performance of the Clark Y is compared with a representative low-Reynolds-numbers airfoil, the S8036. As may be seen, the lifting performance of the Clark Y is superior to the S8036, especially around maximum lift. Both sections display a clockwise hysteresis loop, although the loop is smaller for the S8036 at $Re = 75,000$. The benefit of the S8036 is reflected in a slightly lower drag coefficient at $Re = 150,000$ [based on an equal lift coefficient comparison (not shown)].

Effects of the flap leading-edge angle on the measured lift C_l and drag C_d coefficient are shown in Fig. 3 for $Re = 75,000$ for the constant-chord flaps. Note that the *clean wing* refers to that without any leading-edge-flap attachment. Increasing δ is seen to increase the minimum drag coefficient as well as the lift coefficient for minimum drag in an analogous fashion to camber. Flap deflection shows a positive (equivalent to negative camber) zero-lift shift with little change in the lift-curve slope. Additionally, the setting angle δ of the flap does not appear to have a significant impact on the zero-lift angle-of-attack shift. Although the clean wing clearly shows a clockwise hysteresis loop, hysteresis is not evident with the flap present. Maximum-lift $C_{l\max}$ behavior for the flapped airfoils shows a docile stall followed by an apparent plateau, usually indicative of slowing of the forward movement of the separation point. The appearance of the stall is analogous to long bubble stall observed over thin flat plates. At approximately 22–23 deg AOA, $\delta = 0$ and 20 deg shows a $C_{l\max}$ spike, with lift rapidly increasing by ≈ 0.3. Recurring runs indicated that this behavior was repeatable. As will be elucidated, this behavior may be due to the loss or expansion of a trapped vortex above the flap, such that its movement or growth around the leading edge contributes to lift, but results in a collapse of leading-edge suction. Although $\delta = 50$ deg does not show the lift spike, it shows a higher sustained maximum-lift plateau. The drag polars suggest that while the flaps increase the minimum drag coefficient, the curvature of the polars is diminished, suggestive of reduced lift-dependent (predominantly pressure) drag.

Figure 4 explores the effects of higher Reynolds numbers on the prior flap geometries. Characteristics are seen to be similar to 75,000: the flap eliminates hysteresis and yields a sustained $C_{l\max}$ plateau. The increase in Reynolds number, potentially enabling natural transition for the clean wing, has reduced the drag penalty from plate addition. The effect of δ on the zero-lift angle is more pronounced than at 75,000, with increasing flap angle increasing the zero-lift angle. As opposed to $Re = 75,000$, the lift-curve slope for $\delta = 50$ deg increases compared with the other configurations. The lift spike at AOA $= 23$ deg is still present and slightly more pronounced than at $Re = 75,000$. As may be expected when considering the classical variation of drag coefficient with Reynolds numbers, the presented drag coefficients are reduced compared with $Re = 75,000$ (see Fig. 3). The increase in Reynolds number is not seen to increase $C_{l\max}$ for the clean wing but to delay its attainment to higher incidence and to reduce the size of the hysteresis loop. The lift plot's form and magnitude for the flapped geometries appears similar for the two Reynolds number values evaluated.

The characteristics of planar flaps represented by the constant-chord ($\delta = 0$ deg), triangular, and stepped leading-edge geometries are shown in Figs. 5 and 6 for $Re = 75,000$ and 150,000, respectively. The triangular leading-edge-flap configurations do not show a sustained $C_{l\max}$ peak as seen for the constant-chord flaps, but rather a continual increase in lift coefficient until approximately 23 deg incidence. The triangular flaps also show high-angle-of-attack

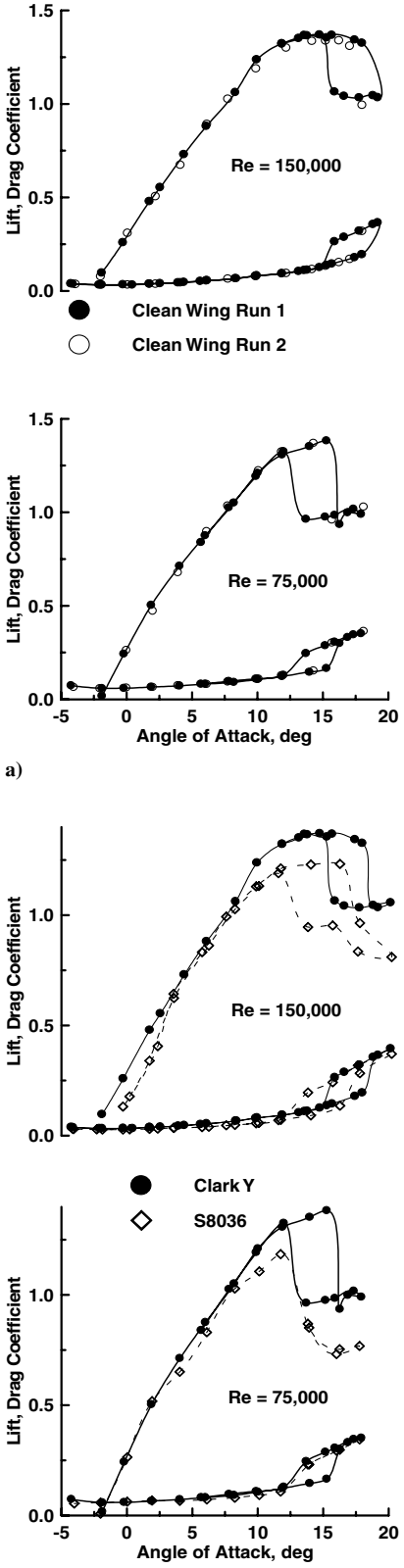

Fig. 2 Plots of a) force-balance repeatability and b) Clark Y performance comparison.

lift production superior to that of the constant-chord flap ($\delta = 0$ deg). Although the lift spike noted for the constant-chord flaps is not present for the triangular flaps, the maximum lift developed by the constant-chord and the triangular flaps at approximately 23 deg AOA is seen to be similar. Figure 5 suggests that the stepped-flap geometry employed was not beneficial. Although the triangular-flap geometries are seen to show favorable

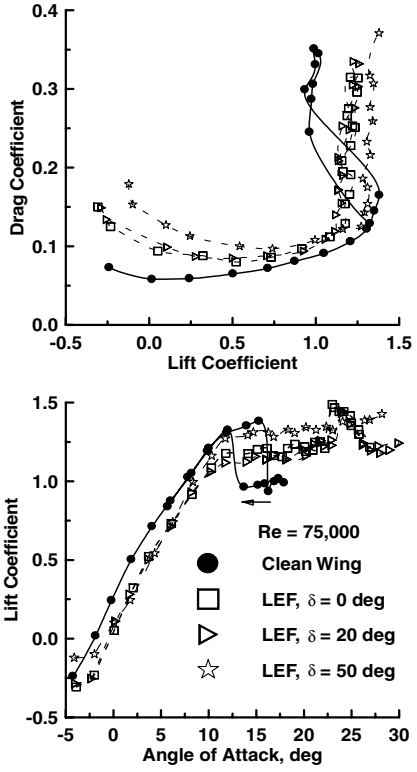

Fig. 3 Effect of constant-chord LEFs on lift and drag coefficient, $Re = 75,000$.

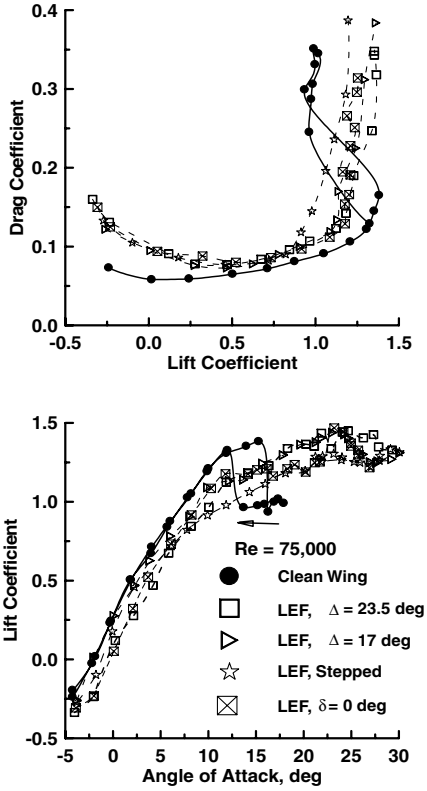

Fig. 5 Effect of variable-chord LEFs on lift and drag coefficient, $Re = 75,000$.

effects compared with the constant-chord flap, differences between the triangular geometries are not clearly apparent. In accord with prior observations, the triangular (and stepped) flaps are seen to eliminate hysteresis. As noted for the deflected flaps (Figs. 3 and 4), increasing Reynolds number to 150,000 reduces the drag penalty associated with flap attachment (Fig. 6). This characteristic is likely associated with a shorter run of laminar flow on the clean wing at $Re = 150,000$, such that possible transition promotion by the flaps would affect the minimum drag coefficient less deleteriously. The increase in Reynolds number results in a observable impact of the

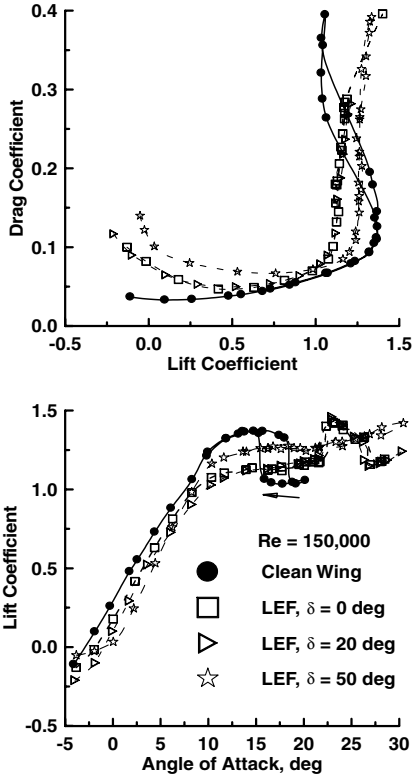

Fig. 4 Effect of constant-chord LEFs on lift and drag coefficient, $Re = 150,000$.

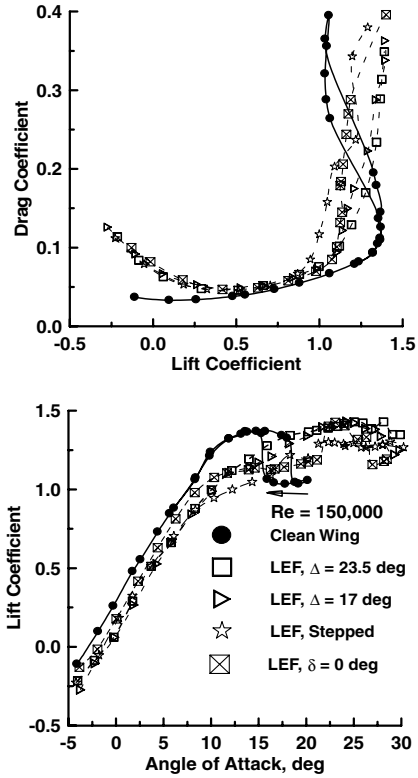

Fig. 6 Effect of variable-chord LEFs on lift and drag coefficient, $Re = 150,000$.

triangular geometry, with the higher-sweep triangles showing greater lift production (than $\Delta = 17$ deg) between 11 and 20 deg AOA. Observed characteristics of hysteresis elimination, absence of the lift spike for triangular and stepped geometries, and inferior behavior of the stepped configuration are evident at $Re = 150,000$. The Reynolds number variation appears to show a minimal impact on the lift produced for a given incidence, as observed for the constant-chord flaps. The triangular geometries also show a positive zero-lift angle-of-attack shift with little discernible difference between $\Delta =$ 17 and 23.5 deg at $Re = 150,000$ (Fig. 6). At lower Reynolds numbers (75,000), the geometry has an effect on the zero-lift incidence shift (Fig. 5).

The ability of the airfoil to generate and sustain leading-edge suction may be investigated through examination of the axial force coefficient $[C_l \sin \text{AOA} - (C_d - C_{d\min}) \cos \text{AOA}]$ presented in Figs. 7 and 8. Also included on the plots is the attainable leading-edge suction (upper inset), which is defined in this paper as the axial force coefficient divided by the maximum axial force ($C_l \sin \text{AOA}$) expressed as a percentage. The parabolic nature of the axial force is clearly apparent. The attainable suction of the clean wing is seen to increase with incidence below stall, whereas the opposite is true for the flap geometries: a consequence of their higher minimum drag coefficient and reduced lift production for a given incidence. The leading-edge flaps yield higher suction levels than the clean wing until stall manifests ($C_l < 1$). This behavior may seem anomalous when viewing the axial force coefficient data, but is a result of the flapped wings producing similar axial force coefficients (for a given incidence) despite having lower C_l than the clean wing for a given incidence. Increasing the flap angle is reflected in an increase in both the axial force and attainable suction. The significant reduction in suction for the flapped configurations for $C_l > 1.1$ is observed to correlate with the onset of the $C_{l\max}$ plateau and large-scale flow separation (and thus pressure drag rise). In most instances, the axial force is similar for all geometries in the attached-flow regime. In the separated-flow regime (AOA > 12 deg), the largest flap angle (50 deg) shows a significant increase in axial force and attainable suction compared with the clean wing at $Re = 75,000$. At $Re = 150,000$, this geometry matches the axial force of the clean

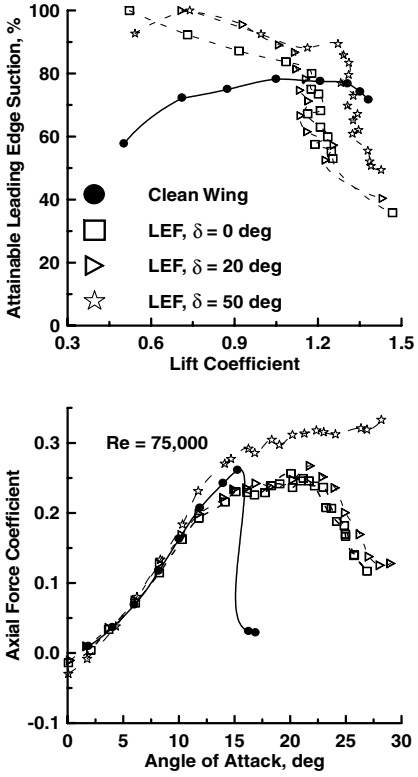

Fig. 7 Effect of constant-chord LEFs on axial force and attainable suction, $Re = 75,000$.

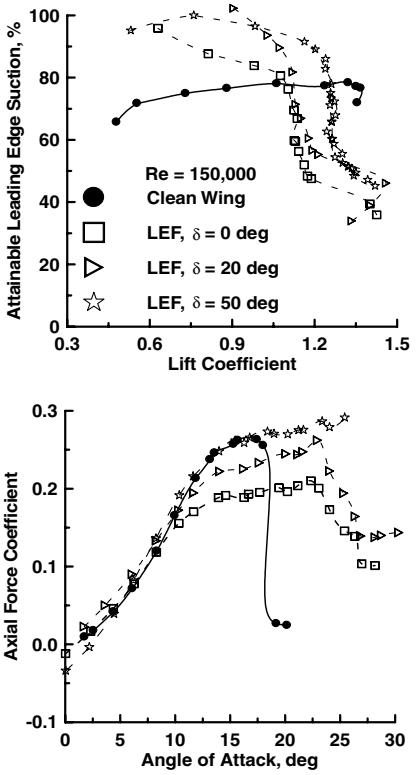

Fig. 8 Effect of constant-chord LEFs on axial force and attainable suction, $Re = 150,000$.

wing, whereas the other flap angles indicate a reduction. The $C_{l\max}$ spike documented earlier (Figs. 3 and 4) for $\delta = 0$ and 20 deg at AOA = 23 deg corresponds to a marked reduction in the axial force coefficient (Figs. 7 and 8). This result suggests that the flap may be losing the suction of a trapped leading-edge vortex, which may reattach on the upper surface near the leading edge or expand onto the upper surface, increasing lift but also greatly reducing the axial force and thus increasing drag. These inferences are also implied in surface pressure traces and flow visualization, discussed later. The increase in the axial force coefficient for $\delta = 20$ deg compared with $\delta =$ 0 deg (Fig. 8) suggests a significant increase in the suction around the leading edge when viewed in concert with the loss of lift for the configuration indicated in Fig. 4. The effect of the flap angle on the axial force produced appears to be minimal between $\delta = 0$ and 20 deg at $Re = 75,000$, but significant at $Re = 150,000$. The axial force developed by the $\delta = 0$ deg flap appears to have diminished at the higher Reynolds number.

The triangular and stepped-flap configurations (see Fig. 9) ($Re = 150,000$ showed similar results) show reduced thrust and suction levels compared with the nonplanar constant-chord leading-edge flap ($\delta = 50$ deg) (see Fig. 7). The stepped geometry indicates significantly degraded performance compared with the other designs. At $Re = 75,000$, the $\Delta = 23.5$ deg triangular flaps demonstrate thrust production superior to $\Delta = 17$ deg. Note that while the triangular flaps do not show the lift spike seen for the constant-chord flaps (Figs. 3–6), they also do not show as significant a loss of axial force as the constant-chord flaps (see Fig. 9).

Analysis of the lift-to-drag ratio (not included, to conserve space) implied that the benefit of the flaps, as implemented in this study, is in the development and sustainability of high-maximum-lift coefficients and elimination of hysteresis, not improvement in range or endurance parameters. The potential advantage of a sustained lift plateau may be controllable and sustainable flight near stall and the minimum flight speed. This could be of value for observation-type missions in which extended loiter over a small geographic region is required.

Jones et al. [7] suggested that the effect of the leading-edge flap in their studies was to behave as a transition device, with this as its likely function in avian application. To explore this, surface pressure traces

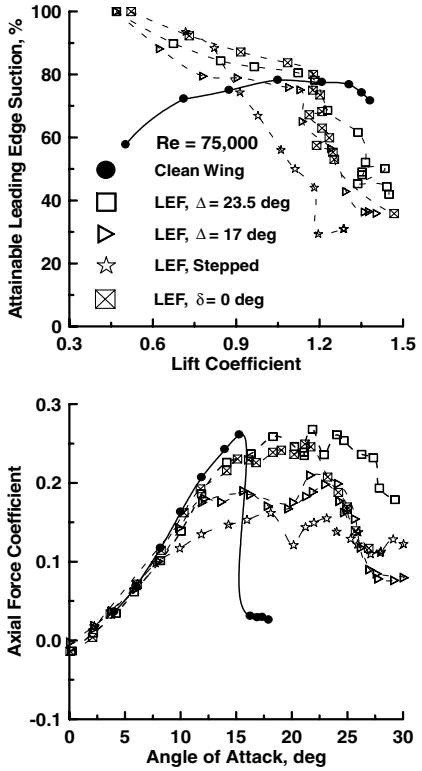

Fig. 9 Effect of variable-chord LEFs on axial force and attainable suction, $Re = 75,000$.

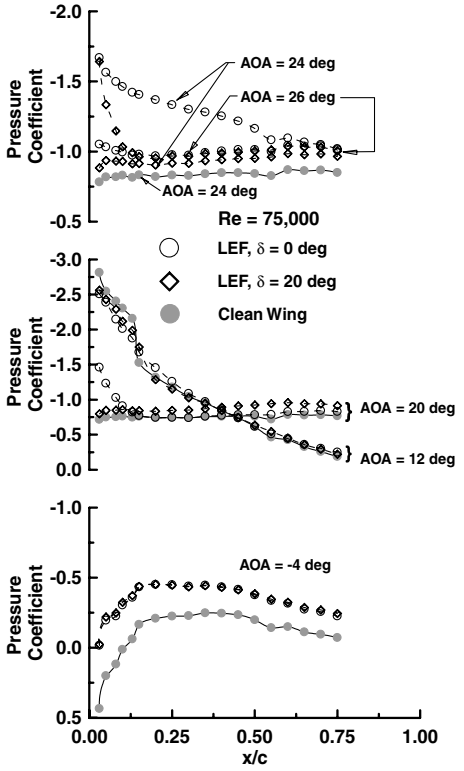

Fig. 11 Measured upper-surface pressure traces for constant-chord LEFs, $Re = 75,000$.

for 0, 4, 8, 12, and 16 deg were analyzed to estimate if a laminar transition bubble was present and, if so, to estimate the transition location. Based on common identification indicators [16], Fig. 10 was assembled. The plot indicates that a bubble was present for all configurations. The increase in Reynolds number is seen to move the transition location forward for all configurations, which is a dependence that is well-documented [1]. The leading-edge flaps do appear to promote a slightly forward movement of transition for AOA ≤ 8 deg. However, they do not appear to act as a transition strip or to promote a significantly earlier occurrence of transition, at least for the tested airfoil–flap combinations.

Surface pressure traces for the clean wing, $\delta = 0$ and 20 deg, are shown in Figs. 11–14. To aid in figure clarity, Figs. 11 and 13 show upper-surface traces and Figs. 12 and 14 show lower-surface plots. For $Re = 75,000$ and AOA $= -4$ deg (Fig. 11), the effect of the flap is seen to be one of increasing the upper-surface suction compared with the clean wing, with the specific flap angle having little effect. However, the flap also causes increased suction on the lower surface (Fig. 12), such that the net effect is increased negative lift at this incidence (see Fig. 3). The lower-surface pressure trace (Fig. 12) does show an effect of the flap angle, with the planar flap indicating the highest suction levels. Similar characteristics are seen at $Re = 150,000$ (Figs. 13 and 14). At an angle of attack of 12 deg, the flaps reduce suction near the leading-edge region compared with the clean wing, until flow reattachment induced by the laminar

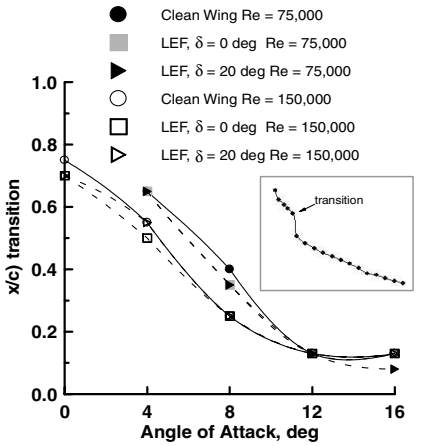

Fig. 10 Estimated location of boundary-layer transition for constant-chord LEFs.

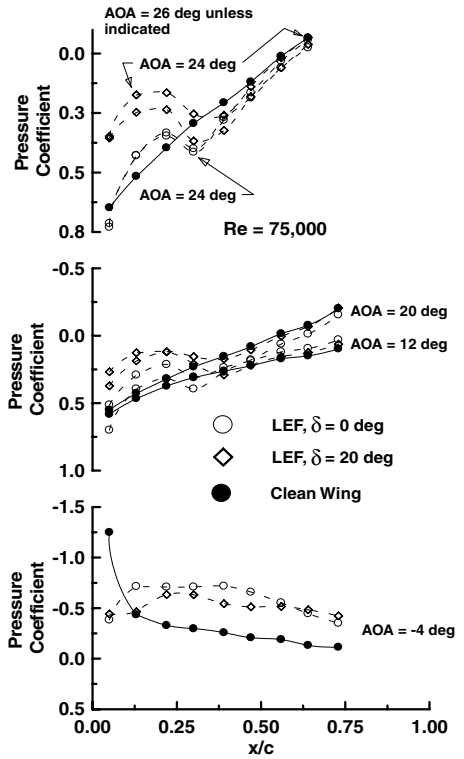

Fig. 12 Measured lower-surface pressure traces for constant-chord LEFs, $Re = 75,000$.

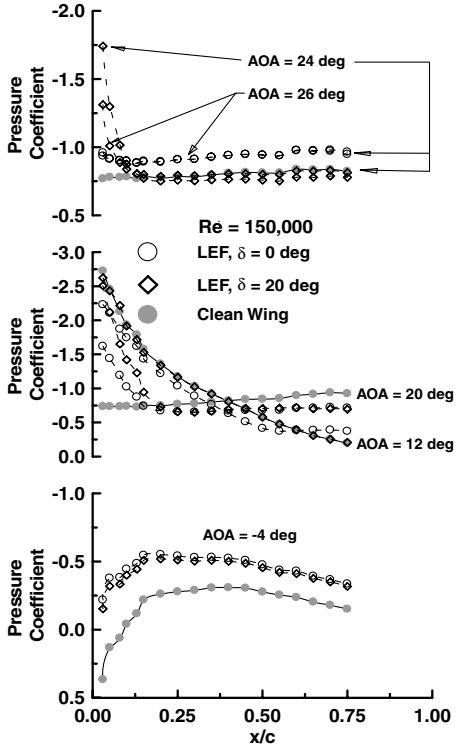

Fig. 13 Measured upper-surface pressure traces for constant-chord LEFs, $Re = 150,000$.

transition bubble on the clean wing reduces surface pressure. A transition bubble is still evident for the configurations with leading-edge flaps (as confirmed by surface-flow visualization), but pressure recovery is less than with the clean wing. Aft of $x/c = 0.3$, the flaps have little indicated effect. For these conditions, the lower-surface pressures are significantly affected by the presence of the flaps forward of $x/c = 0.35$. The flaps reduce the lower-surface pressure (less positive) with $\delta = 20$ deg, showing a reduction larger than

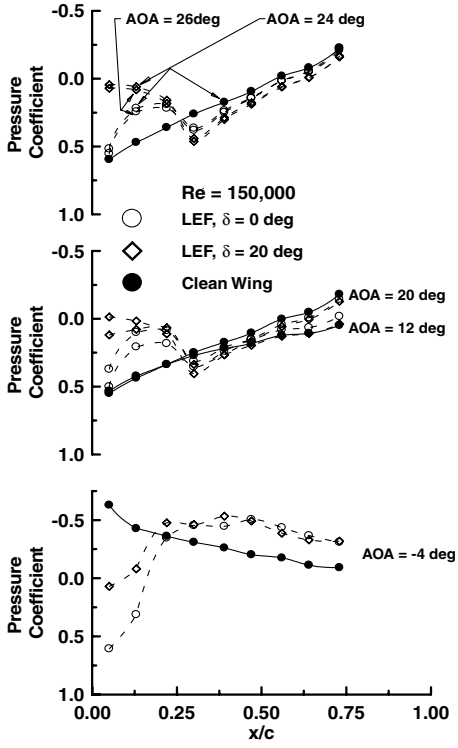

Fig. 14 Measured lower-surface pressure traces for constant-chord LEFs, $Re = 150,000$.

$\delta = 0$ deg (Fig. 12). The upper-surface distribution taken in concert with that of the lower surface suggests that the reduction in pressure on the lower-surface forward airfoil section is primarily responsible for the loss of lift compared with the clean wing. Reynolds number does appear to have a small impact on the traces, as may be observed in Figs. 13 and 14. The upper-surface trace for the clean wing and $\delta = 20$ deg are seen to be similar, whereas that for $\delta = 0$ deg indicates a loss of suction compared with the aforementioned wings and possible separation from approximately 60% chord aft (Fig. 13). The lower-surface traces (Fig. 14) show flap effects similar to those noted for $Re = 75,000$ with little impact aft of 35% chord, but the flaps decrease the lower-surface pressure over the forward wing section and thus, ultimately, the integrated lift coefficient.

At AOA $= 20$ deg, most traces show massive upper-surface flow separation ($Re = 75,000$, Fig. 11). Note that $\delta = 0$ deg does indicate attached-type flow on the upper surface until about 10% chord. Lower-surface pressure shows trends similar to those at AOA $= 12$ deg (Fig. 12). Increasing the Reynolds numbers to 150,000 shows attached-flow forward suction distributions for both flap geometries until approximately 25% chord, and the lower-surface traces are similar to those at $Re = 75,000$. At an angle of 24 deg incidence (Fig. 11, $Re = 75,000$), the clean wing shows a flat trace, which is typically associated with massive separation. The traces for the flapped wings show the reestablishment of partially-attached-flow surface distributions over the upper airfoil surface. This reestablishment corresponds to the observed lift spike, as noted in Figs. 3 and 4. The upper-surface pressure trace for $\delta = 0$ deg at 24 deg incidence (Fig. 11) shows what appears to be mostly attached upper-surface flow. This attached extent was not verified or observed using surface-flow visualization and should consequently be treated with caution. Similar but less pronounced characteristics are seen at $Re = 150,000$. Additionally, the lower-surface pressure traces show a positive shift with respect to the clean wing for $x/c > 0.25$ contributing toward lift production for both $Re = 75,000$ and 150,000. At $Re = 150,000$, $\delta = 0$ deg does not show a significant leading-edge suction peak as noted at lower Reynolds numbers, or for $\delta = 20$ deg at both Reynolds numbers, but shows a higher constant suction level over most of the upper surface. Furthermore, the lower-surface trace suggests less lift loss over the forward airfoil section compared with $\delta = 20$ deg. The reestablishment of partially attached flow may be a consequence of a movement or expansion of a trapped leading-edge vortex (as suggested by prior axial force data). The relocation or expansion of this vortex onto the upper surface may increase lift as well as aid in flow reattachment.

As mentioned, the leading-edge flaps may not initiate significantly earlier transition, as has been suggested [7]. Note that the different geometries of the flaps in this investigation and [7] may be responsible for the observed differences. This may be a result of the shear layer that separates from the plate edge convecting through a highly favorable pressure region, potentially leading to stretching of the shear layer and thus inhibiting the formation of Kelvin–Helmholtz instabilities. Additionally, this shear layer may roll up to form a trapped vortex above the flap. As a result, the fluid that reattaches on the upper airfoil surface would not propagate from the flap's shear layer.

It was observed during recording of the pressure traces that while the traces were pseudosteady for the clean configuration at stalled conditions, the leading-edge flap's (LEF's) data showed an apparently stochastic cycling, from massively separated to attached in the leading-edge vicinity. A data series, where pressures were recorded at 1 s intervals, yielded Fig. 15. The symbol shading intensity is consistent with time progression. As may be seen, the flow is seen to cycle (and would repeat the sequence shown) and may be indicative of the instability of the leading-edge vortex after its migrated or expanded, with the vortex forming and then advecting downstream. Note that the sequence displayed was not consistent: the trace sometimes showed massive separation for approximately 5 to 10 s, followed by a rapid suction-peak establishment and then collapse.

To support the notion of a migrating or expanding leading-edge vortex as well as corroborate the pressure signatures (in the inference

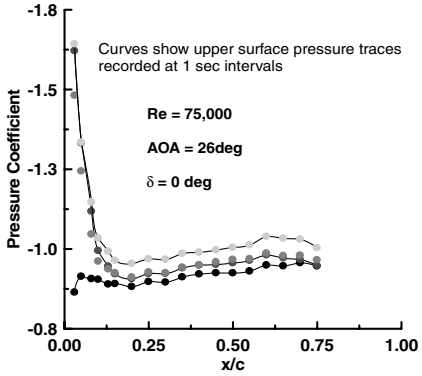

Fig. 15 Temporal variation of measured upper-surface pressure trace, $Re = 75,000$.

that the LEFs may not initiate transition), surface-flow visualization was undertaken. Recorded skin-friction patterns are shown in Figs. 16 and 17. Images for the clean wing are shown in Fig. 16. An incidence of 12 deg shows a leading-edge transition bubble for both Reynolds numbers. Although not clearly apparent (especially for $Re = 75,000$, there is little energy in the flow to move the paint mixture), observation during the tests indicated massive upper-surface separation for both Reynolds numbers at 24 deg angle of attack.

Figure 17 shows images for the constant-chord flap with $\delta = 0$ deg. Angles of attack are presented to bracket the observed lift spikes as well as to support the notion that the flaps may not cause transition. As may be seen, supporting the pressure data, the constant-chord flap does not appear to promote transition, such that a laminar bubble is still present near the leading edge for AOA $= 12$ deg. The trailing-edge separation at this incidence visible for $Re = 150,000$ is also reflected in the surface pressure trace (Fig. 13). The bubble appears to show streamwise striations or a sawtooth pattern near its leading edge, which is a characteristic often identified with a crossflow instability [17]. These are a result of the formation of small streamwise vortices within the boundary layer [17]. As the airfoils were unswept, this is unlikely to be the mechanism responsible but may be indicative of a three-dimensional character of the separating shear layer. Note that the flap appears to show pooling of the paint, suggestive of localized separation. This would imply that the leading-edge stagnation point is below the flap. At 24 deg incidence, the

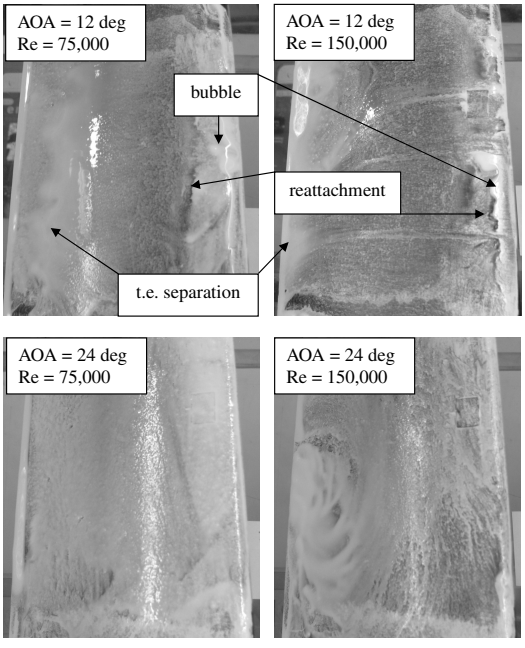

Fig. 16 Surface skin-friction patterns over the clean wing.

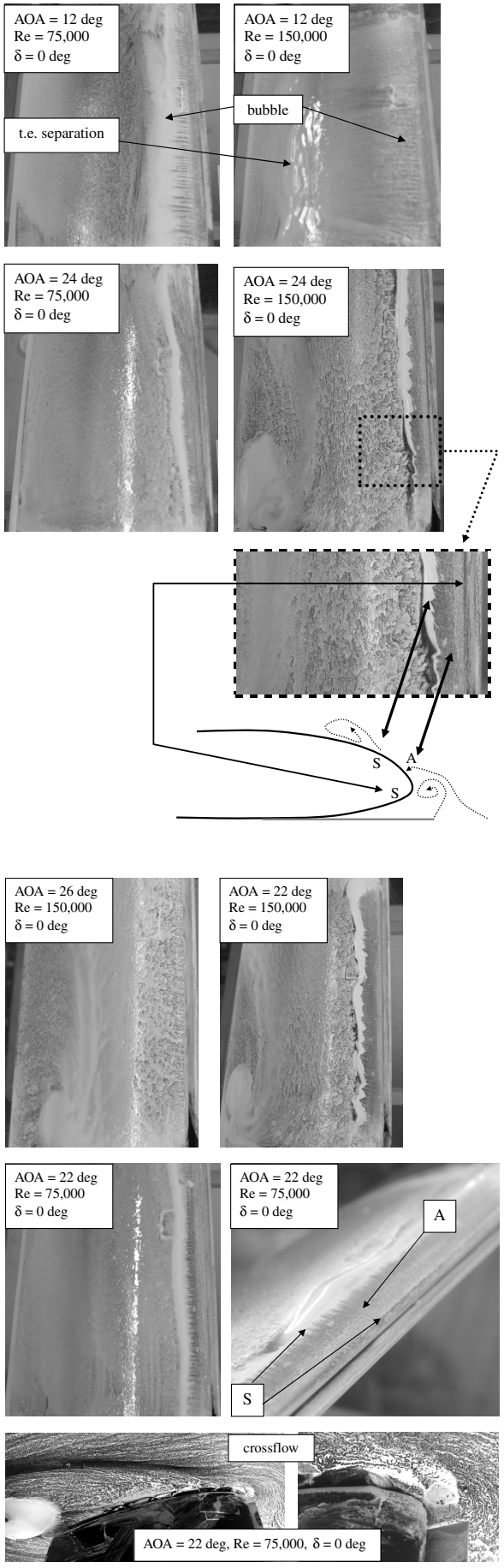

Fig. 17 Surface skin-friction patterns over the constant-chord flapped wing, $\delta = 0$ deg.

presence of a region of leading-edge attached flow is indicated, as suggested by the pressure traces. A likely interpretation of the leading-edge topology is shown in the lower inset of Fig. 17. *A* and *S* refer to attachment and separation, respectively. Similar images are present at 22 deg incidence, along with a rendering of the crossflow skin-friction lines (lower inset). The presence of a leading-edge vortex type structure is evident above the flap. Examination of the images for AOA = 22 and 24 deg reveals similar leading-edge topology, but of different scale. At AOA = 22 deg, the attached-flow extent is approximately 38% larger than at AOA = 24 deg. Note that 22 deg incidence corresponds to the peak of the lift spike, whereas at 24 deg the lift spike has attenuated but is still present. Consequently, the surface patterns suggest the notion that the leading-edge vortex grows and then diminishes in size, with its maximum extent over the upper surface, corresponding to the lift spike. Its growth, with the concomitant reduction in suction applied near the leading edge (from geometric considerations) causes a loss of axial force and an increase of lift. At 26 deg incidence (top left inset), the surface flow shows massive separation with the loss of leading-edge attached flow.

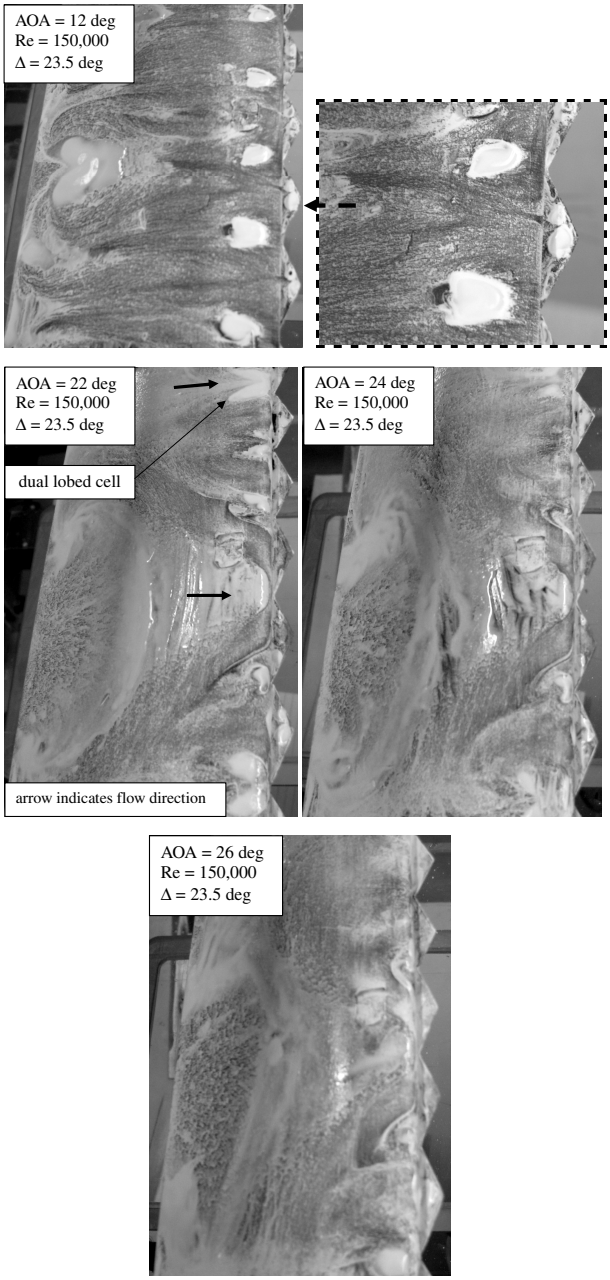

Fig. 18 Surface skin-friction patterns over the flapped wing, Δ = 23.5 deg.

To gain insight into the physics differentiating the high-incidence behavior of the constant-chord and triangular flaps, surface skin-friction images were visualized for Δ = 23.5 deg at angles of attack similar to those of the constant-chord flapped wings. The images are presented in Fig. 18. At 12 deg incidence, the presence of the flaps is seen to have the effect of splicing the laminar bubble into sections, with the remaining bubble segments located at the valley between adjacent triangles. On the triangular flaps, two recirculating separation cells are visible. A separation line appears to emanate from the triangular flap's center region and propagate streamwise over the upper surface (observation during the test showed fluid periodically being expelled from the bubbles on the flaps and running streamwise, leaving the darker visible separation lines). At this incidence, 12 deg, the flow appears to be attached over the forward 55% of the chord. The trailing-edge region indicates large extents of separated flow. The patterns with this flap are seen to be vastly different from those with the constant-chord flap (Fig. 17). It is unclear if the splicing of the laminar bubble is due to the triangular plates generating coherent vortical streamwise structures or if they are effective at promoting boundary-layer transition (or a combination of both).

At higher incidence, 22 deg and above, the flow shows large regions of trailing-edge separation (see Fig. 18). The leading-edge region shows separated dual-lobed separation cells at the valley between the triangular-flap segments. Flow observation during testing showed that fluid from the trailing edge flowed upstream and terminated in the lobed structures. The skin-friction patterns indicate regions of attached and separated flow, with the attached regions generally located behind the triangular flap's apex region. Even at 26 deg, regions of attached flow are still evident. As opposed to the constant-chord flaps, the surface images do not show any large topological changes in this incidence range, reflected in the smooth and continuous lift behavior discussed earlier. At 22, 24, and 26 deg, separation lines are seen to run spanwise and then approximately streamwise from the flap vicinity. Closer image observation indicates skin-friction lines with a strong sidewash orientation that may be suggestive of vortical formation. However, if the triangular flaps do create leading-edge vortices, the flaps' very low sweep may mitigate against formation of stable vortices. The flaps may generate vortical structures that help initiate transition. Gad-el-Hak and Blackwelder [18] have observed the formation of Kelvin–Helmholtz type instabilities in the leading-edge shear layer over moderate-sweep delta wings at low Reynolds numbers.

Conclusions

A two-dimensional low-speed wind-tunnel investigation was conducted to evaluate the effect of lower-surface leading-edge flaps. The flaps consisted of a thin plate that was attached to the pressure side of a Clark Y airfoil section. Various flap angles and geometries were investigated. Testing was undertaken at two Reynolds numbers: 75,000 and 150,000. Performance characterization included force balance, pressure measurement, and flow visualization. Results indicated that the flap appeared to decamber the airfoil, shifting the zero-lift angle of attack in the positive direction. An increase in the minimum drag coefficient with flap attachment yielded a reduction in the achievable lift-to-drag ratio compared with the unmodified wing. Benefits of the flap are evident at high incidence: the flap shows a sustained maximum-lift plateau as opposed to a clearly identifiable stall for the unmodified airfoil. As the flaps degrade performance at low-to-moderate lift coefficients, potential implementation in a flight vehicle would require them to be deployable. For practical use, the flaps would need to be compared with other flow control devices such as vortex generators, which may be structurally simpler. Some flap configurations showed a marked lift spike at approximately 22–23 deg incidence, which was associated with a significant drop in the axial force coefficient and leading-edge suction. It was surmised that the spike may be due to the enlargement or movement of a trapped leading-edge vortex formed above the flap. Surface pressure traces indicated that the largest contributor to the loss of lift associated with the flaps was caused by a reduction in lower-surface pressure over the

forward extent of the airfoil. Although hysteresis was present over the unmodified airfoil, the application of the flaps eliminated it. It has been suggested that the function of such a flap in avian application may be to act as a transition device; surface-flow images showed that a laminar transition bubble was still present after flap attachment. Surface visualization also showed the presence of a spanwise-orientated leading-edge vortex for some of the flap configurations.

Acknowledgments

The authors would like to thank Praful Chowdri, Michael Dewey, and Robert Williams for manufacturing the wings used in this study and performing the force-balance testing. The authors would also like to thank the Associate Editor and reviewers for their helpful comments and suggestion.

References

[1] Traub, L. W., and Cooper, E., "Experimental Investigation of Pressure Measurement and Airfoil Characteristics at Low Reynolds Numbers," *Journal of Aircraft*, Vol. 45, No. 4, 2008, pp. 1322–1333. doi:10.2514/1.34769

[2] Selig, M. S., and Guglielmo, G., "High Lift Low Reynolds Number Airfoil Design," *Journal of Aircraft*, Vol. 34, No. 1, 1997, pp. 72–79. doi:10.2514/2.2137

[3] Liebeck, R., "Laminar Separation Bubbles and Airfoil Design at Low Reynolds Numbers," AIAA Applied Aerodynamics Conference, 10th, AIAA Paper 1992-2735, Palo Alto, CA, June 22–24, 1992.

[4] Kerho, M., Hutcherson, S., Blackwelder, R. F., and Liebeck, R. H., "Vortex Generators Used to Control Laminar Separation Bubbles," *Journal of Aircraft*, Vol. 30, No. 3, 1993, pp. 315–319. doi:10.2514/3.46336

[5] Eppler, R., *Airfoil Design and Data*, Springer–Verlag, Berlin, 1990.

[6] Traub, L. W., and Moeller, B., "Low-Reynolds-Number Effects on Delta-Wing Aerodynamics," *Journal of Aircraft*, Vol. 35, No. 4, 1998, pp. 653–656. doi:10.2514/2.2352

[7] Jones, A. R., Baktian, N. M., and Babinsky, H., "Low Reynolds Number Aerodynamics of Leading-Edge Flaps," *Journal of Aircraft*, Vol. 45, No. 1, 2008, pp. 342–345. doi:10.2514/1.33001

[8] Zhang, H. J., and Zhou, Y., "Leading-Edge Surface-Manipulated Flow Separation from an Airfoil," *Journal of Aircraft*, Vol. 45, No. 6, 2008, pp. 2171–2173. doi:10.2514/1.36998

[9] Wong, C. W., and Rinoie, K., "Bubble Burst Control for Stall Suppression on a NACA 631-012 Airfoil," *Journal of Aircraft*, Vol. 46, No. 4, 2009, pp. 1465–1476. doi:10.2514/1.43924

[10] Lissaman, P. B. S., "Low-Reynolds-Number Airfoils," *Annual Review of Fluid Mechanics*, Vol. 15, 1983, pp. 223–239. doi:10.1146/annurev.fl.15.010183.001255

[11] Seshagiri, A., Traub, L. W., and Cooper, E., "Effects of Vortex Generators on an Airfoil at Low Reynolds Numbers," *Journal of Aircraft*, Vol. 46, No. 1, 2009, pp. 116–122. doi:10.2514/1.36241

[12] Mueller, T. J., "The Influence of Laminar Separation and Transition on Low Reynolds Number Airfoil Hysteresis," *Journal of Aircraft*, Vol. 22, No. 9, 1985, pp. 763–770. doi:10.2514/3.45199

[13] Traub, L. W., "Efficient Lift Enhancement of a Blunt Edged Delta Wing," *The Aeronautical Journal*, Nov. 1997, pp. 439–445.

[14] Rinoie, K., and Stollery, J., "Experimental Studies of Vortex flaps and Vortex Plates," *Journal of Aircraft*, Vol. 31, No. 2, 1994, pp. 322–329. doi:10.2514/3.46490

[15] Rao, D. M., and Johnson, T. D., Jr., "Investigation of Delta Wing Leading Edge Devices," *Journal of Aircraft*, Vol. 18, No. 3, 1981, pp. 161–167. doi:10.2514/3.57479

[16] Popov, A. V., Botez, R., M., and Labib, M., "Transition Point Detection from the Surface Pressure Distribution for Controller Design," *Journal of Aircraft*, Vol. 45, No. 1, 2008, pp. 23–28. doi:10.2514/1.31488

[17] Poll, D. I. A., "On the Effects of Boundary Layer Transition on a Cylindrical After-Body at Incidence in Low-Speed Flow," *The Aeronautical Journal*, Oct. 1985, pp. 315–327.

[18] Gad-el-Hak, M., and Blackwelder, R. F., "The Discrete Vortices from a Delta Wing," *AIAA Journal*, Vol. 23, No. 6, 1985, pp. 961–962. doi:10.2514/3.9016